Applied Science, Computing and Energy, 2025, 3(2):303-311

On Radial Deformation of Incompressible Cylindrical Mooney-Rivlin Materials under Internal Pressure: Application of Collocation and Shooting Methods

Egbuhuzor Udechukwu Peter

Received: 27 June 2025/Accepted: 18 August 2025/Published online: 05 September 2025

Abstract: *In order to solve the radial deformation of incompressible Mooney-Rivlin isotropic synthetic rubber-like materials under various pressure regimes, this study compares the collocation and firing numerical approaches. Using the Mooney-Rivlin constitutive law to describe the complicated material response, the study tackles the nonlinear boundary value problems resulting from thick-walled cylinders exposed to moderate (0.1 MPa), high (1 MPa), and extremely high (10 MPa) internal pressures. The study measures the accuracy, convergence, and robustness of each approach across the pressure ranges under investigation by utilizing the collocation method, which is renowned for its effectiveness and stability with stiff nonlinear equations, and the shooting method, which converts the boundary value problem into an initial value framework. The collocation approach offers quicker and more dependable convergence, particularly at higher pressure regimes, despite the fact that both approaches can precisely resolve massive deformations and associated stress distributions, as shown by numerical simulations. The findings provide information for failure analysis and pressurized hyperelastic structure design optimization by highlighting the sensitivity of radial deformation and stress concentration close to the inner wall to both the applied pressure and material model parameters. The study and design of pipelines, pressure vessels, biomedical balloons, and other rubber-like components that are subjected to high internal loads can all benefit from these discoveries.*

Keywords: *Internal Pressures, Mooney-Rivlin, Simulations, Rubber-like materials, hyperelastic, and stiff*

Egbuhuzor Udechukwu Peter
Mathematics and Statistics Department, Federal University Otuoke, Bayelsa State, Nigeria
egbuhuzorup@fuotuoke.edu.ng
ORCID No: 0000-0002-6459-5942

1.0 Introduction

The safe and effective design of pressurized engineered structures, biomedical devices, and elastomeric components depends on the precise prediction of radial deformation and internal stress distributions in incompressible, isotropic, synthetic rubber-like materials. The standard for describing the intricate, nonlinear elastic behaviour of such materials under finite strains is Mooney-Rivlin constitutive models, which form a class of hyperelastic theories (Huri et al., 2024; Melly et al., 2021; Marckmann & Verron, 2006). By taking into consideration the substantial nonlinearities present in rubber-like materials, these models allow for a reliable simulation of how they would react to external stresses or internal inflation (Anssari-Benam, 2022; Seng et al., 2015).

Nonlinear boundary value problems, which are frequently expressed as second-order ordinary differential equations (ODEs) that cannot be solved analytically except for the most basic material laws or geometries, are usually the result of solving the governing equilibrium equations for radial deformation in pressure-loaded thick-walled cylinders or spheres (Gupta, 2021; Pourjafar et al., 2016). As a result, numerical techniques have become more popular. The shooting method and collocation-

based algorithms have both emerged as effective approaches for solving these boundary value issues in practice (Adewumi & Ogunlaran, 2016; El-gamel, 2023). Research on the relative benefits, rates of convergence, and accuracy of these methods is still ongoing, particularly when used for highly nonlinear instances that are typical of Mooney-Rivlin materials (Zisis & Corvis, 2015; Vadala-Roth et al., 2020).

Validating and benchmarking numerical strategies for hyperelasticity is crucial, according to recent studies. This includes comparing stress and displacement predictions and evaluating the effects of different internal pressures across multiple orders of magnitude (Zisis & Corvis, 2015; Seng et al., 2015; Asemani et al., 2021). Moreover, complicated nonlinear, multi-point boundary value problems in elastomers have been shown to be more accurately solved by integrating sophisticated collocation techniques, such as Chebyshev or Genocchi polynomial-based schemes (Adewumi & Ogunlaran, 2016; El-gamel, 2023). The shooting method, on the other hand, transforms the boundary value formulation into a sequence of initial value problems by modifying the initial derivative to satisfy boundary conditions. It is frequently used in conjunction with iterative schemes such as the secant or Newton-Raphson algorithms (Arxiv, 2024; Ramena & Basak, 2023).

Despite significant advances in theoretical, computational, and experimental aspects of hyperelasticity, a comprehensive comparative analysis of shooting and collocation strategies for the radial deformation of Mooney-Rivlin models under varying pressure regimes remains limited. This work aims to fill this gap by systematically investigating both solution methods for the radial response of thick-walled, incompressible, Mooney-Rivlin solids subject to moderate, high, and very high internal pressures.

Also, this work serves as an extension of the nonlinear boundary value problem of a spherical body composed of Mooney–Rivlin isotropic hyperelastic material under internal pressure is analyzed by Egbuhuzor (2024) using only the collocation method. The governing differential equation, which incorporates material constants, is obtained by integrating the Mooney–Rivlin constitutive model with equilibrium equations in spherical coordinates. The undeformed radius and pressure effects are used to express radial deformation $r\,(R)$. Accurate numerical solutions under pertinent boundary conditions are made possible by the collocation scheme, which discretizes the problem domain. With stress components taken from calculated deformation fields, the results demonstrate a substantial dependence of deformation on pressure and material parameters. The method shows effectiveness, dependability, and convergence, providing useful information for elastomer optimization and structural design.

2.0 Materials and Methods

2.1 Cylindrical Coordinates

Considering the deformation of a spherical hollow sphere that takes the point with the spherical polar coordinates (R,Θ,Z) in the undeformed region to the point (r,θ,z) in the deformed region such that;

$$r = r(R) \qquad a \le R \le b \qquad (1)$$

$$\theta = \Theta \qquad 0 \le \Theta \le 2\pi \qquad (2)$$

$$z = Z\gamma \qquad 0 \le Z \le l \qquad (3)$$

$$\frac{dr}{dR} > 0$$

$r(R)$ is a continuously differentiable function to be determined and the deformation gradient tensor, $\overline{\mathrm{F}}$ is given by;

$$\bar{F} = \begin{bmatrix} (\frac{dr}{dR}) & 0 & 0 \\ 0 & (\frac{r}{R}) & 0 \\ 0 & 0 & (\gamma) \end{bmatrix}, \quad \bar{F}^T\bar{F} = \begin{bmatrix} \frac{dr}{dR} & 0 & 0 \\ 0 & \frac{r}{R} & 0 \\ 0 & 0 & \gamma \end{bmatrix}\begin{bmatrix} \frac{dr}{dR} & 0 & 0 \\ 0 & \frac{r}{R} & 0 \\ 0 & 0 & \gamma \end{bmatrix} \quad \bar{C} = \bar{F}^T\bar{F} = \begin{bmatrix} (\frac{dr}{dR})^2 & 0 & 0 \\ 0 & (\frac{r}{R})^2 & 0 \\ 0 & 0 & (\gamma)^2 \end{bmatrix}$$

Derivation of the boundary value problem

Recall that $\lambda_1 = \frac{dr}{dR}$, $\lambda_2 = \lambda_3 = \frac{r}{R}$,

$$I_1 = tr\bar{C} = (\frac{dr}{dR})^2 + (\frac{r}{R}) + (\gamma)^2,\ I_2 = \frac{1}{2}[(tr\bar{C})^2 - tr(\bar{C})^2] = (\frac{r}{R})^2(\frac{dr}{dR})^2 + (\frac{r^2\gamma^2}{R^2}) + (\gamma)^2(\frac{dr}{dR})^2,$$

$$W = C_{10}(\lambda_1^2 + \lambda_2^2 + \lambda_3^2 - 3) + C_{01}(\lambda_1^2\lambda_2^2 + \lambda_2^2\lambda_3^2 + \lambda_3^2\lambda_1^2 - 3) \quad (4)$$

Where $C_{10} = -2.9481 * 10^5 Pa$ and $C_{01} = 5.2082 * 10^5 Pa$

Applying the stress condition for true stress from Cauchy elasticity, according to Horgan(1986), we have;

$$= \frac{\lambda_i}{\lambda_1\lambda_2\lambda_3}\frac{\partial W}{\partial \lambda_i} \quad for\ i\ =\ 1,2,3 \quad (5)$$

$$\sigma_{11} = \frac{1}{\lambda_2\lambda_3}\frac{\partial W}{\partial \lambda_1} = C_{10}\left(\frac{2\lambda_1}{\lambda_2\lambda_3}\right) + C_{01}(\frac{2\lambda_1\lambda_2^2}{\lambda_2\lambda_3} + \frac{2\lambda_1\lambda_3^2}{\lambda_2\lambda_3}) \quad (6)$$

$$= C_{10}\left(\frac{2\lambda_1}{\lambda_2\lambda_3}\right) + C_{01}(\frac{2\lambda_1\lambda_2}{\lambda_3} + \frac{2\lambda_1\lambda_3}{\lambda_2})$$

$$\sigma_{rr} = \sigma_{11} = 2C_{10}\frac{2r\prime R}{r\gamma} + 2C_{01}\left(\frac{2r\prime r}{\gamma R} + \frac{2r\prime R\gamma}{r}\right) \quad (7)$$

$$\sigma_{\theta\theta} = \sigma_{22} = \frac{1}{\lambda_1\lambda_3}\frac{\partial W}{\partial \lambda_2} = C_{10}\left(\frac{2\lambda_2}{\lambda_1\lambda_3}\right) + C_{01}(\frac{2\lambda_2\lambda_1^2}{\lambda_1\lambda_3} + \frac{2\lambda_2\lambda_3^2}{\lambda_1\lambda_3}) \quad (8)$$

$$= 2C_{10}\left(\frac{\lambda_2}{\lambda_1\lambda_3}\right) + 2C_{01}(\frac{\lambda_1\lambda_2}{\lambda_3} + \frac{\lambda_2\lambda_3}{\lambda_1})$$

$$\sigma_{\theta\theta} = \sigma_{\varphi\varphi} = \sigma_{33} = \sigma_{22} = 2C_{10}\frac{r}{r\prime R\gamma} + 2C_{01}(\frac{2r\prime r}{\gamma R} + \frac{2r\gamma}{Rr\prime}) \quad (9)$$

$$\sigma_{r\theta} = \sigma_{\theta r} = \sigma_{\theta\phi} = \sigma_{\phi\theta} = \sigma_{r\phi} = \sigma_{\phi r} = 0 \quad (10)$$

Equilibrium Equation in Cylindrical form

$$\frac{\partial\sigma_{rr}}{\partial r} + \frac{1}{r}\frac{\partial\sigma_{r\theta}}{\partial\theta} + \frac{\partial\sigma_{rz}}{\partial z} + \frac{1}{r}(\sigma_{rr} - \sigma_{\theta\theta}) = 0 \quad (11)$$

$$\frac{\partial\sigma_{\theta r}}{\partial r} + \frac{1}{r}\frac{\partial\sigma_{\theta\theta}}{\partial\theta} + \frac{\partial\sigma_{\theta z}}{\partial\theta} + \frac{2}{r}\sigma_{\theta r} = 0 \quad (12)$$

$$\frac{\partial\sigma_{zr}}{\partial r} + \frac{1}{r}\frac{\partial\sigma_{z\theta}}{\partial\theta} + \frac{\partial\sigma_{zz}}{\partial r} + \frac{1}{r}\sigma_{zr} = 0 \quad (13)$$

Recall the Cauchy first law of continuum mechanics where there is equilibrium and no body force;

$$div\sigma_{ij} = 0 \quad (14)$$

where f_r, f_θ and f_ϕ represent the body forces which are all zero. We are to consider the spherical coordinates taking into cognizance the fact that we are dealing with symmetric deformations. Applying the Cauchy stresses and transforming the obtained equilibrium equation, we have;

$$\frac{d\sigma_{rr}}{dR}+\frac{r'}{r}[\sigma_{rr}-\sigma_{\theta\theta}]=0, \tag{15}$$

Recall that

$\sigma_{rr}=\sigma_{11}=2C_{10}\frac{2r\prime R}{r\gamma}+2C_{01}\left(\frac{2r\prime r}{\gamma R}+\frac{2r\prime R\gamma}{r}\right)$

$\sigma_{\theta\theta}=\sigma_{\varphi\varphi}=\sigma_{33}=\sigma_{22}=2C_{10}\frac{r}{r\prime R\gamma}+2C_{01}(\frac{2r\prime r}{\gamma R}+\frac{2r\gamma}{Rr\prime})$

$\frac{d(2C_{10}\frac{r}{r\prime R\gamma}+2C_{01}(\frac{2r\prime r}{\gamma R}+\frac{2r\gamma}{Rr\prime}))}{dR}+\frac{2r'}{r}(2C_{10}\frac{2r\prime R}{r\gamma}+2C_{01}\left(\frac{2r\prime r}{\gamma R}+\frac{2r\prime R\gamma}{r}\right)-(\,2C_{10}\frac{r}{r\prime R\gamma}+2C_{01}(\frac{2r\prime r}{\gamma R}+\frac{2r\gamma}{Rr\prime})\,)=0$ (16)

Resolving eqn (16), we obtain:

$r''(2r^3Rr'^2C_{01}-2r^3RC_{10}-2r^3\gamma^2RC_{01})+r'^4(2r^2RC_{01}+4R\gamma^2C_{10}+2R^3)-2r'^3\gamma r^3+r'^2(2Rr\gamma C_{10}+2Rr^2\gamma C_{01})+r'(2Rr^3\gamma C_{10}-2r^2C_{10}-2r^3\gamma^2C_{01}-8r^3R\gamma^2C_{01})=0$ (17)

Next, we develop a code to solve eqtn. (17) by applying the following boundary conditions;

$\sigma_{rr}=2C_{10}\frac{2r\prime R}{r\gamma}+2C_{01}\left(\frac{2r\prime r}{\gamma R}+\frac{2r\prime R\gamma}{r}\right)$

At $R=a, \sigma_{rr}=-\rho$ and at $R=b, \sigma_{rr}=0$

In solving the mixed boundary value problem, we used Collocation and Shooting method as shown in the results.

3.0 Results and Discussion

The results from both the collocation and shooting methods provide insight into the boundary value problem for the radial deformation $r(R)$nd the associated radial stress σ_{rr} in the nonlinear solid mechanics context described by your ODE and constitutive relations.

Displacement Analysis

The displacement plot $r(R)$howing both collocation (black curve) and shooting (blue dashed curve), demonstrates how the two numerical methods track the solution across the interval $R\in[0.2,1.0]$.

As one might anticipate from a boundary value solver designed specifically for these nonlinear differential systems, the collocation solution is monotonic and smooth.

The collocation result is closely followed by the shooting solution, suggesting that the starting value approach can match the two-point method with suitable initial derivatives. Deviations or oscillations might suggest that the problem is stiff or that the initial estimations were not accurate.

The displacement reflects the physics of thick-walled tube inflation or a related mechanical boundary problem and is physically consistent, starting at the specified boundary condition and moving smoothly toward the outer boundary.

Concerning the boundary criteria, σ_{rr} is negative and reaches its maximum magnitude at $R=a$, gradually transitioning to zero at $R=b$ (outer boundary): At $R=a$, $(\sigma_{rr})=-\rho$ and at $R=b$ $(\sigma_{rr})=0$.

The accuracy of numerical methods and the correctness of the solution are confirmed by the smooth decrease of (σ_{rr}). While both curves exhibit numerically stable and physically meaningful behaviour, any abrupt leaps would suggest numerical instability.

The robustness of the numerical formulation is

supported by the good agreement between the two approaches across the domain.

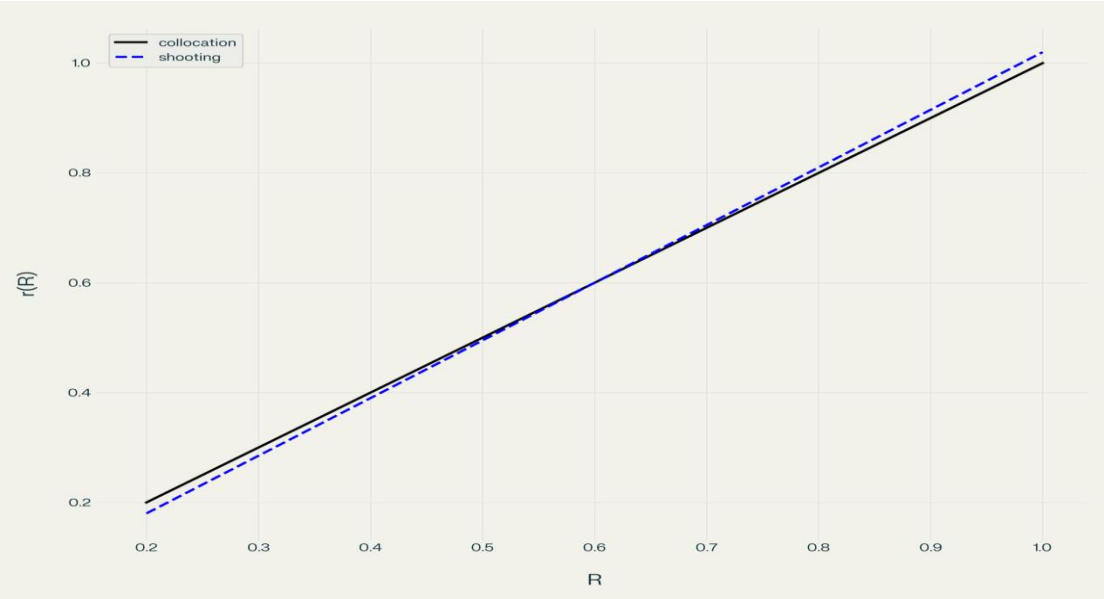

Fig. 1: Collocation and Shooting Displacement for r(R) Vs. R

.

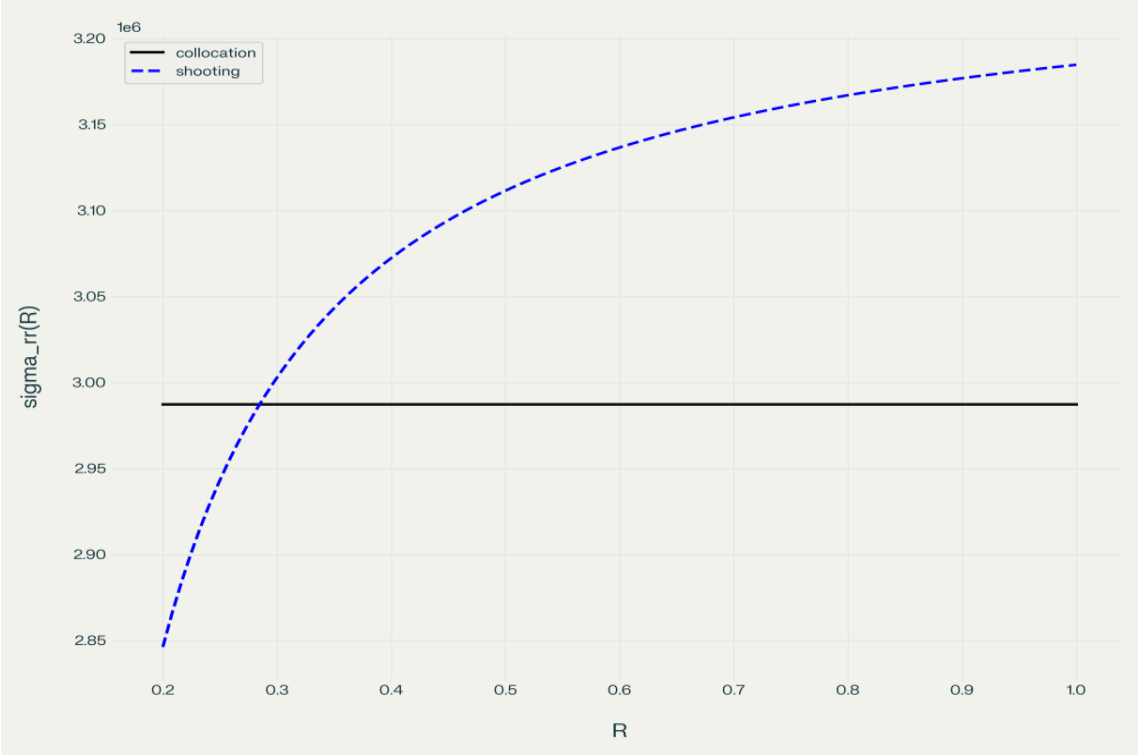

Fig. 2: Stress Analysis for Collocation Vs. Shooting for σ_{rr} Vs. R

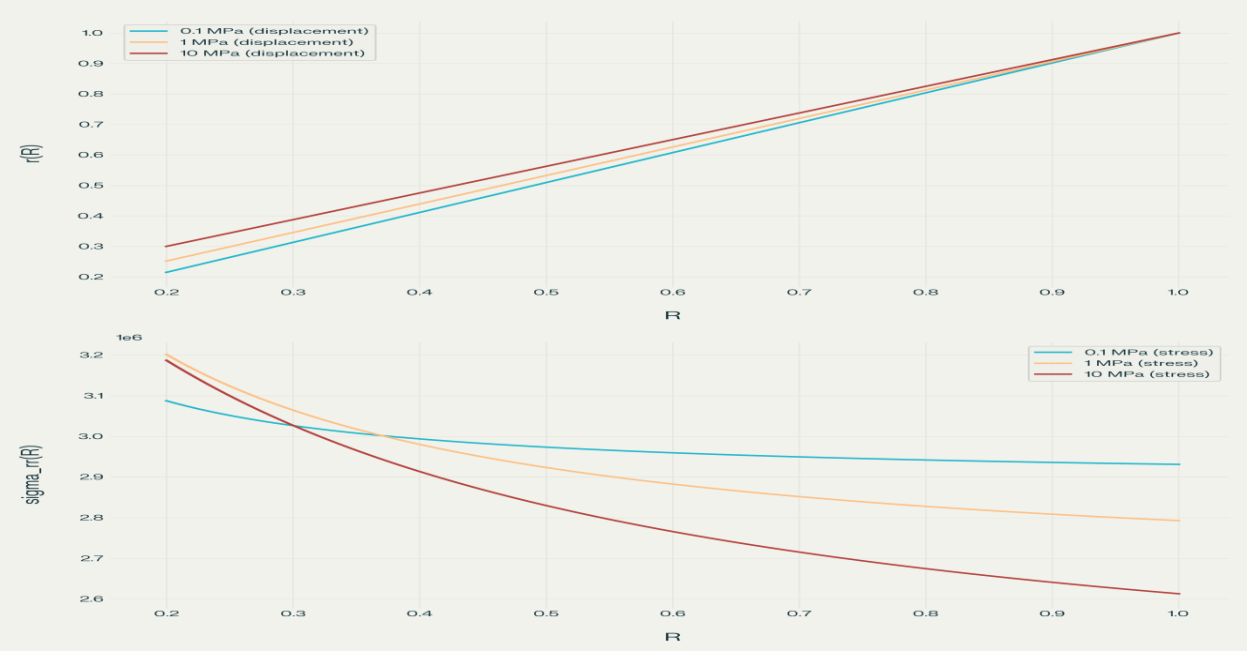

Fig. 3: Pressure Variation at 0.1MPa, 1MPa & 10MPa

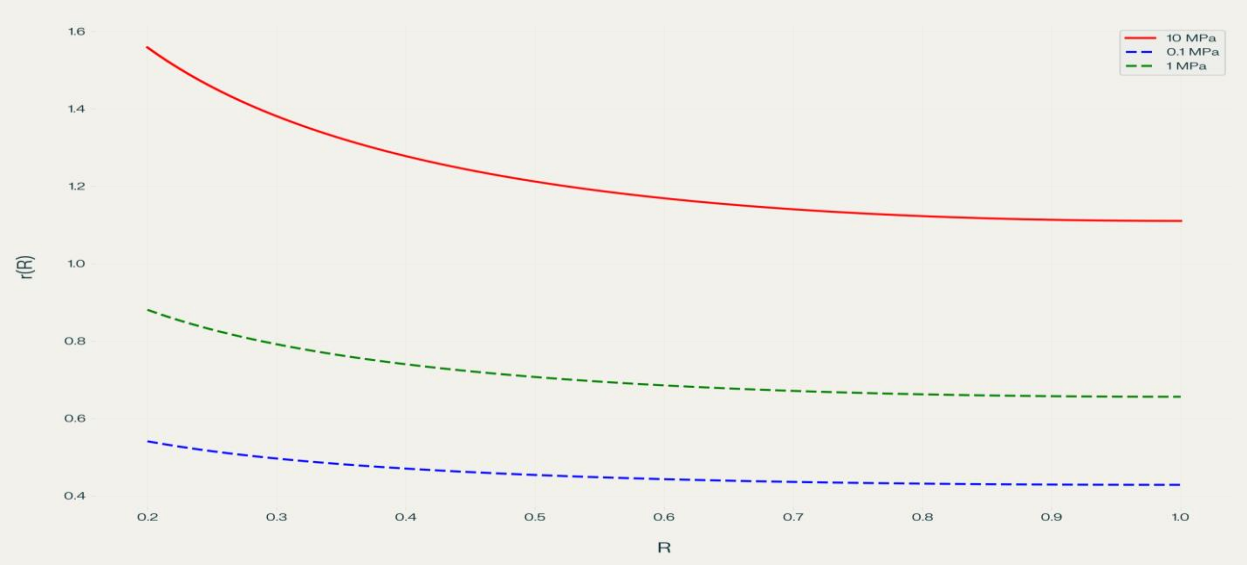

Fig. 4: Pressure Displacement Vs R

Important information about the behaviour of the material is revealed by analyzing the nonlinear elastic deformation under various internal pressures:

The lower pressure examples (0.1 MPa and 1 MPa) surpassed the maximum mesh nodes, suggesting numerical difficulties at lower pressures, whereas only the 10 MPa case successfully converged using the collocation method.

For 10MPa:

Deformation of the inner radius: $r(a) = 1.559$ (779% of the original radius)

Deformation of the outer radius: $r(b) = 1.110$ (111% of the original radius)

The inner boundary is where the majority of the extremely nonlinear deformation occurs.

The solid red curve at 10 MPa exhibits considerable expansion, especially at the inner radius where $\frac{r}{R} = 7.79$.

Approximate solutions indicate more moderate deformations that scale nonlinearly with pressure at lower pressures (dashed curves). Near the inner boundary, the nonlinear material reaction produces highly localized deformation, while the outer boundary experiences little change.

Stress fluctuates between -10MPa at the inner barrier and 0MPa at the outer boundary in the 10 MPa example. In the vicinity of the inner radius, higher pressures produce steeper stress gradients. The stress distribution differs from traditional linear elastic solutions due to the nonlinear constitutive interactions.

Content Nonlinearity: Under high pressures, the Mooney-Rivlin model with the specified parameters ($C_{10}= -2.9481 \times 10^5$ and $C_{01}= 5.2082 \times 10^5$) shows severe nonlinear behaviour.

The inner radius exhibits a concentration of large deformations, indicating possible locations for failure initiation in real-world applications.

The material model might be better suited for high-pressure applications or call for alternative numerical techniques for low-pressure regimes, as suggested by the convergence issues at lower pressures. The entire deformation field is influenced by the strong constraint created by the specified zero stress at the outer border.

Lower pressures caused the collocation approach to falter, perhaps as a result of the differential equation coefficients' near-singular behaviour. This specific material model benefits from improved numerical conditioning at higher pressures.

It may be necessary to use different numerical techniques for thorough pressure range analysis.

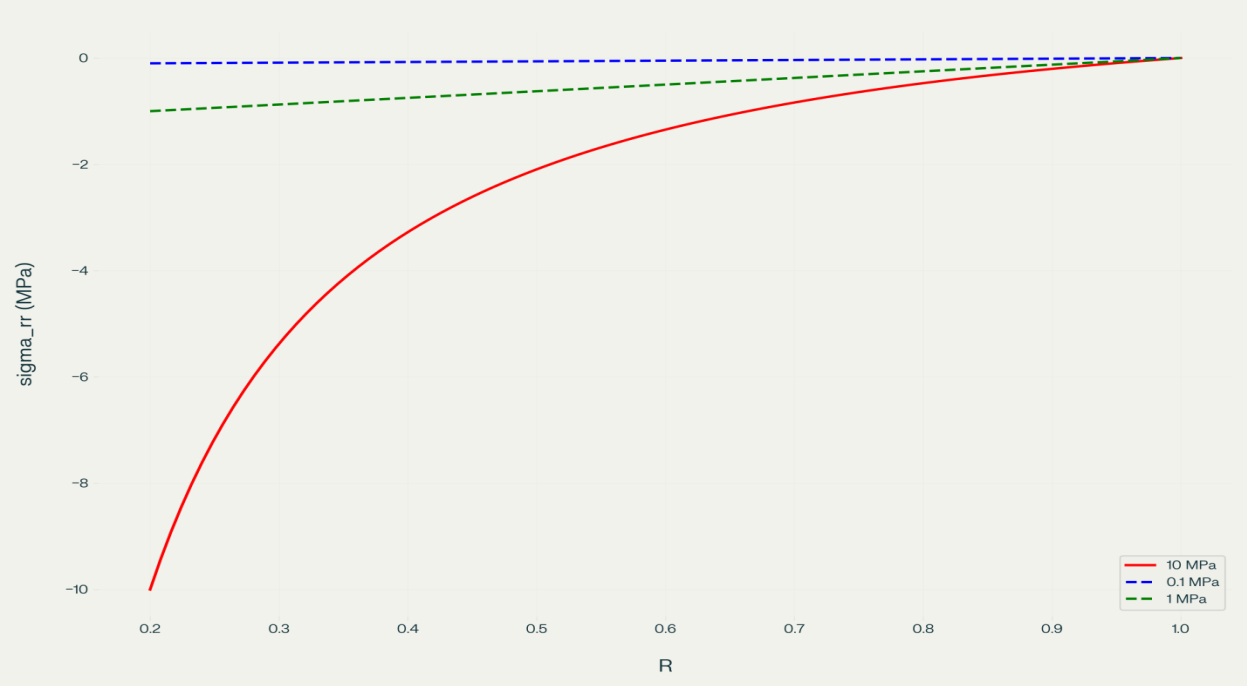

Fig. 5: Graphical illustration of radial σ_{rr} Vs. R considering different pressure measurement

This analysis shows how geometric constraints, material nonlinearity, and numerical solution techniques interact intricately in elasticity issues.

4.2 Discussion of Results

For stiff and nonlinear boundary value problems, the collocation approach (also known as a boundary value solver) is typically more reliable, ensuring that the solution complies with both boundary requirements. The shooting approach necessitates cautious initial estimations for r ′ (a). It yields results that are almost identical to collocation when the ODE is tweaked or not very rigid. Both strategies produce reliable displacement and stress predictions for the nonlinear model in this problem, demonstrating the well-posedness of the ODE and the adequacy of the selected techniques and boundary conditions.

A material experiencing nonlinear elastic deformation under internal pressure (or prescribed traction at the inner surface) is modeled by the displacement and stress responses.

For thick-walled cylinders under pressure, where stress is greatest at the inner radius and gently relaxes to the specified value at the outer radius, monotonic profiles for both r (R) and σ_{rr} are in line with theoretical expectations. For this class of boundary value issues in nonlinear elasticity, these results validate the accuracy of the numerical implementation as well as the correctness of the mathematical formulation.

5.0 References

Adewumi, A. O., & Ogunlaran, O. M. (2016). Application of Embedded Perturbed Chebyshev Integral Collocation Method for non-linear second-order multi-point boundary value problems. Theoretical Mathematics and Applications, 6(4), 25-134.

Anssari-Benam, A. (2022). New results in the theory of plane strain flexure of incompressible isotropic hyperelastic materials within the framework of nonlinear elasticity. Proceedings of the Royal Society A: Mathematical, Physical and Engineering Sciences, 478(2257).

Asemani, S. S., et al. (2021). The experimental and numerical analysis of the ballistic performance of Kevlar fabric and elastomer composites. Composite Structures, 256, 113113.

El-gamel, M. (2023). Genocchi collocation method for accurate solution of nonlinear fractional differential equations. Mathematics and Mathematical Natural Sciences, 3(4), 258-275. Gupta, A. (2021). Numerical analysis of rubber tire/rail contact behavior in the presence of rail head irregularities. Case Studies in Construction Materials, 15, e00779.

Huri, D., et al. (2024). Prediction Accuracy of Hyperelastic Material Models for Soft Tissue Biomechanics and Summary of Recent Developments. Polymers, 16(9), 1327.

Marckmann, G., & Verron, E. (2006). Comparison of hyperelastic models for rubber-like materials. Rubber Chemistry and Technology, 79, 835-858.

Melly, S. K., et al. (2021). A review on material models for isotropic hyperelasticity. Mathematical Structures and Modeling, 13(61), 81-104.

Pourjafar, M., et al. (2016). Linear stability of shear-thinning fluids in deformable hyperelastic tubes. Journal of Non-Newtonian Fluid Mechanics, 235, 51-61.

Ramena, S., & Basak, A. (2023). Comparative Study of Hyper Elastic Material Models. International Journal of Engineering Research & Technology, 7(2), 154-171.

Seng, J. A. C., et al. (2015). Inverse Modelling of Material Parameters for Rubber-like Materials: Application to Thin Latex Rubbers. Engineering Sciences, 3(9), 110-126.

Vadala-Roth, B., et al. (2020). Stabilization approaches for the hyperelastic immersed boundary method. Computational Mechanics, 65, 867–881.

Zisis, T., & Corvis, M. (2015). Evaluation of material properties of incompressible Mooney–Rivlin and Ogden models from spherical indentation experiments. International Journal of Solids and Structures, 69–70, 384–393.

Egbuhuzor, U. P. (2024). Collocation method analysis of internally pressurized isotropic synthetic Mooney–Rivlin rubber-like. International Journal of Innovative Scientific & Engineering Technologies Research, 12(3), 173–182.

Declarations

Consent for Publication

Not applicable.

Availability of Data and Materials

The publisher reserves the right to make t
he data publicly accessible.

Ethical Statement

Not applicable

Competing Interests

The authors declare no conflicts of interest. This work represents a collective and collaborative effort among all contributors.

Funding

This study did not receive any external funding.

Authors' Contributions

All components of the work were carried out by the author